A Quasi-Static Analysis for a Class of Induced-Current EIT Systems Using Discrete Coils

Adnan Köksal*, *Member, IEEE*, B. Murat Eyüboğlu, *Member, IEEE*, and Mehmet Demirbilek

***Abstract*—A discrete coil EIT system is investigated for the general case of an eccentric circular inhomogeneity. The solution methodology of the forward problem of this system is explained. An optimization procedure using this forward problem solution is developed to find optimum currents that maximize the distinguishability. For an eccentric inhomogeneity problem, it is shown that the coil currents can be optimized to focus the current density in a region of interest. Optimum coil currents under limited peak coil currents constraint and limited total power constraint are obtained. Representative examples that demonstrate the performance of the system are presented.**

***Index Terms*—Conformal tranformation, discrete coil, distinguishability, electrical impedance tomography, induced-current EIT, optimum current pattern.**

I. Introduction

ELECTRICAL impedance tomography (EIT) is an imaging modality first employed in geophysics, later developed as a medical imaging modality within the last 25 years [1]. EIT reconstructs the absolute conductivity distribution or variations in conductivity distribution based on electrical measurements performed on the surface of a conductor [2], [3]. Based on the method of current application to the conductor, EIT systems can be classified as injected or induced-current systems. In injected-current EIT, current is injected through an array of electrodes (e.g., 16 or 32 electrodes) along the boundary of the object and measurement of voltage at the electrodes helps the determination of an image representing the conductivity distribution. Induced-current EIT [4]–[8] works with similar principles, the main difference being the induction of the current using a coil or coils located outside the object.

In EIT systems, independent measurements of potential at the boundary are used to form an image of the object [2], [3]. In order to obtain independent potential distributions, the induced current in the object must be changed in an independent manner. In injected-current EIT systems, this is accomplished by changing the drive electrode position, whereas in single-coil induced-current EIT systems, the location of the coil with respect to the object is changed for the same purpose. Koksal *et al.* [9] proposed a discrete coil structure and an optimum coil excitation scenario for induced-current EIT systems. In a discrete coil system, the location of the coils does not have to be changed, the drive current of the coils may be changed instead for increased number of independent measurements and improved sensitivity.

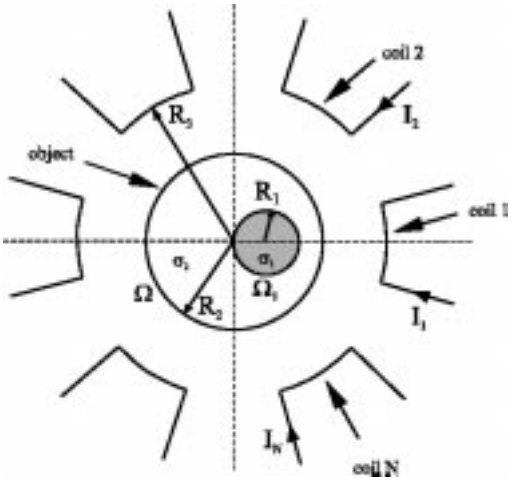

Fig. 1. Discrete coil EIT configuration.

In this paper, a discrete coil EIT system is investigated for the general case of an eccentric circular inhomogeneity, for the first time. The analysis is carried out using a quasi-static assumption and by neglecting the displacement field in the object. For the concentric inhomogeneity case only, formulation for continuous single- and multiple-coil cases is given in [7] and [8], and for discrete coils it is given in [10]. Section II gives the forward problem solution for an eccentric inhomogeneity. Distinguishability analysis for this problem is given in Section III, where the the problem of finding the best coil currents is cast into a constrained nonlinear optimization problem. Section IV gives some representative results of forward analysis and of distinguishability optimization under two different constraints. Conclusions are presented in Section V.

II. Method of Analysis

Consider the problem geometry shown in Fig. 1 which displays a two-dimensional circular object of conductivity σ_2 with an eccentric circular inhomogeneity of conductivity σ_1 and radius R_1. The boundary of the inhomogeneity is Ω_1 and of the object is Ω which coincides with $r = R_2$. At $r = R_3$, the

Manuscript received August 20, 2001; revised February 22, 2002. *Asterisk indicates corresponding author.*

*A. Köksal is with the Hacettepe University, Electrical and Electronics Engineering Department, Ankara 06532, Turkey, (e-mail: koksal@hacettepe.edu.tr)

B. M. Eyüboğlu is with the Middle East Technical University, Electrical and Electronics Engineering Department, Ankara 06531, Turkey.

M. Demirbilek is with the Hacettepe University, Electrical and Electronics Engineering Department, Ankara 06532, Turkey.

Publisher Item Identifier 10.1109/TMI.2002.800603.

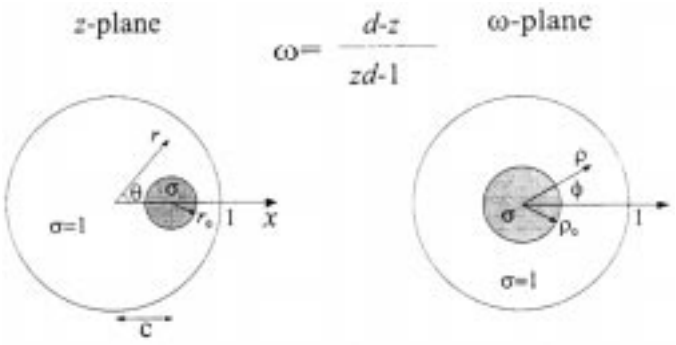

Fig. 2. The conformal transformation $\omega = (d-z)/(zd-1)$ transforms the original eccentric inhomogeneity problem of (a) in z plane ($z = re^{j\theta}$) to the concentric problem of (b) in ω plane ($\omega = \rho e^{j\phi}$).

coils of the system are located with each coil consisting of an angular sector and two radial arms. This simple mathematical model successfully simulates a coil geometry which is closed in the transverse plane of the investigated body. Throughout numerical experiments that will be presented, effect of the radial arms has been seen to be negligible and in practical realization the radiation by them can be suppressed using a solenoidal winding on a ferrite. The problem can be solved efficiently using a quasi-static assumption which neglects the secondary effects. In other words, the total magnetic field is assumed to be that of the primary coil magnetic fields, and the secondary effect of the electric field on the magnetic field is negligible.

In the frequency regime of conventional EIT, the conducting properties of objects are much more pronounced than the dielectric properties. This fact constitutes the second approximation used, i.e., $\sigma \gg \omega\epsilon$.

Using the two previously stated assumptions for the problem of Fig. 1, and denoting the solution for potential within the inhomogeneity by Φ_1, and outside the inhomogeneity by Φ_2, the equation to be solved becomes

$$\nabla^2\Phi = 0 \tag{1}$$

with boundary conditions

$$\left.\frac{\partial\Phi_2}{\partial r}\right|_{r=R_2} = -\omega A_n(R_2) \tag{2}$$

$$\left.\left(\sigma_2\frac{\partial\Phi_2}{\partial n} - \sigma_1\frac{\partial\Phi_1}{\partial n}\right)\right|_{z\in\Omega_1} = -(\sigma_2-\sigma_1)\omega A_n \tag{3}$$

$$\Phi_1 = \Phi_2 \text{ on } \Omega_1. \tag{4}$$

In (1)–(4), $\partial/\partial n$ represents the normal derivative, z denotes any point in the problem geometry and A_n is the normal component of the primary vector magnetic potential on Ω_1. The potentials in these equations are actually the imaginary parts of the potentials; the real parts can be shown to be identically zero under the given assumptions [7].

The conformal transformation [11] shown in Fig. 2 converts the original problem of Fig. 2(a) where a circular inhomogenity of radius r_0 and conductivity σ centered at $x = c$ to the concentric problem of Fig. 2(b) where the inhomogeneity radius becomes ρ_0. The parameters related to the conformal transformation shown in Fig. 2 are given as

$$\rho_0 = \frac{\left[1-c^2+r_0^2-\sqrt{(1-c^2+r_0^2)^2-4r_0^2}\right]}{2r_0} \tag{5}$$

$$d = \frac{\left[1+c^2-r_0^2-\sqrt{(1+c^2-r_0^2)^2-4c^2}\right]}{2c}. \tag{6}$$

Under this conformal transformation the Laplacian operator in two dimensions is invariant and, therefore, the problem in the transform plane can be solved easily using concentric theory. The solution in the original problem domain is then obtained using back-transformation. It is important to note here that the coil geometry is not affected by the conformal transformation. If we consider (2)–(4), we see that the normal component of the primary magnetic vector potential appears only as a source term. Therefore, the effect of the magnetic vector potential can be viewed as an effective current density existing at the boundaries of the problem. One of the differences of induced-current EIT from injected-current EIT is that the effective current density exists not only at the outer boundary, but also at the inhomogeneity boundary. In order to complete the tranformation of the problem to ω plane the boundary conditions which shows the effect of primary magnetic field must also be transformed properly. These boundary conditions are transformed to the transform (ω) plane [11] using

$$A_n[\phi(\theta)] = \frac{A_n(\theta)}{|w'(z)|_{z\text{ on }\Omega\text{ or }\Omega_1}}. \tag{7}$$

A Fourier analysis solution for the potential in the transform plane can be affected provided that the scalar line integral around any closed-contour C of the normal component of vector potential is zero in the cross-sectional plane, i.e.,

$$\int_C \bar{A}\cdot\overline{dl} = 0. \tag{8}$$

While it is known that the Coulomb's gauge, $\nabla\cdot\bar{A} = 0$, is satisfied for all loops of steady current, note that (8) is satisfied by a class of these loops which generate equal amounts of field lines entering and leaving the object at the cross-sectional plane. It is worth mentioning here that, although the results given in this paper are for the coil geometry of Fig. 1, the analysis that will follow will be applicable to all coil geometries that satisfy (8).

Under the approximations stated up to now, the electrostatic potential in the transform (ω) plane can be written as

$$\Phi_1(\rho,\phi) = \sum_{m=1}^{\infty}\rho^m(e_m\cos(m\phi) + f_m\sin(m\phi)) \tag{9}$$

$$\Phi_2(r,\phi) = \sum_{m=1}^{\infty}\left(\rho^m a_m + \rho^{-m}b_m\right)\cos(m\phi) + \left(\rho^m c_m + \rho^{-m}d_m\right)\sin(m\phi). \tag{10}$$

Unknown coefficients in (9) and (10) can be found as

$$a_m = \frac{1}{2}\left[(1+\alpha)e_m + (1-\alpha)\frac{1}{\rho_1^{m-1}}E_m\right] \tag{11}$$

$$b_m = \frac{1}{2}\left[(1-\alpha)\rho_1^{2m} e_m - (1-\alpha)\rho_1^{m+1} E_m\right] \quad (12)$$

$$c_m = \frac{1}{2}\left[(1+\alpha) f_m + (1-\alpha)\frac{1}{\rho_1^{m-1}} F_m\right] \quad (13)$$

$$d_m = \frac{1}{2}\left[(1-\alpha)\rho_1^{2m} f_m - (1-\alpha)\rho_1^{m+1} F_m\right] \quad (14)$$

$$e_m = \frac{2\beta^m C_m - [(1-\alpha)+(1-\alpha)\beta^{2m}]\beta E_m}{\beta^m R_2^{m-1}[(1+\alpha)-(1-\alpha)\beta^{2m}]} \quad (15)$$

$$f_m = \frac{2\beta^m D_m - [(1-\alpha)+(1-\alpha)\beta^{2m}]\beta F_m}{\beta^m R_2^{m-1}[(1+\alpha)-(1-\alpha)\beta^{2m}]} \quad (16)$$

where $\alpha = \sigma_1/\sigma_2$ and $\beta = \rho_1/R_2$, ρ_1 being the radius of the inhomogeneity in the transform plane, and

$$C_m = -\frac{\omega}{\pi m}\int_0^{2\pi} A_n(R_2,\phi)\cos(m\phi)d\phi \quad (17)$$

$$D_m = -\frac{\omega}{\pi m}\int_0^{2\pi} A_n(R_2,\phi)\sin(m\phi)d\phi \quad (18)$$

$$E_m = -\frac{\omega}{\pi m}\int_0^{2\pi} A_n(\rho_1,\phi)\cos(m\phi)d\phi \quad (19)$$

$$F_m = -\frac{\omega}{\pi m}\int_0^{2\pi} A_n(\rho_1,\phi)\sin(m\phi)d\phi. \quad (20)$$

It is seen that if $\bar{A}$ is known for the given coil configuration, the solution for potential Φ in the transform plane is readily obtained in terms of the Fourier coefficients of the transformation of A_n which is obtained using (7). The numerical solution of the problem is based on the truncation of the Fourier series for the vector potential. The vector potential and its normal component at the boundaries are calculated for the chosen geometry as given in [10]. Considering Fig. 1, the contribution from the angular sector of coils is found using numerical integration. The calculation for the radial segments of coils is carried out analytically. As a result, the forward problem is solved as follows.

1) $A_n(\phi)$ is calculated at the boundaries using numerical integration. For this purpose, K equally separated points are chosen in the transform plane and $A_{n1}(\phi)$ and $A_{n2}(\phi)$ are calculated for each of the N coils. During this calculation, the locations of these points in the original (z) plane are found and (8) is utilized. The calculation is repeated for each coil and A_{n1} and A_{n2} are stored as $K \times N$ matrices.
2) Truncated Fourier series coefficients for both A_{n1} and A_{n2} are calculated and C_m, D_m, E_m, and F_m are found. These are stored as $M \times N$ arrays where M is the required number of terms in Fourier series. Note that the latter is simply related to the Fourier coefficients by the multiplicative constant $-(\omega/m)$. Here, the required number of terms is determined dynamically by checking the error between respective A_n and its Fourier sum. 1% error bound between the two yields satisfactory results. Contrary to the concentric inhomogeneity case, the number of Fourier coefficents needed is not very small and increases as the inhomogeneity gets closer to the object boundary.
3) The potential in the transform plane is calculated using (9) and (10) and it is back-transformed to the original plane.
4) If current density in the object is required, the magnetic vector potential is calculated where the current is required. Note that this is done totally in the original coordinates since the coil geometry is not affected by the transformation. The second current density component requires the calculation of $\nabla\Phi$. This calculation is carried out in the transform plane at the images of the required points, and the back transform is found using the chain rule of differentiation.

III. Distinguishability Analysis

Distinguishability of an EIT system is defined by Isaacson [12] as the system's ability to detect the conductivity difference of an inhomogeneity from the background. How well the system is able to do so is mathematically expressed as the difference of the norm of potential at the boundary for the cases where the inhomogeneity is and is not present. Best currents that maximize the distinguishability are studied in [12] and [13] under constant power constraint for the injected-current EIT. Later, the effect of constraints on the distinguishability performance of the system is studied in [15], where it is shown that while cosine drive is better under constant power constraint, opposite drive has a better distinguishability when the total current injected to the object is kept constant. Opposite drive has been shown to be actually the best under constant injected-current constraint in [16] using an optimization procedure. Later, appropriate electrical safety constraints and the optimal current patterns under these constraints are discussed in [17].

Consider again the problem shown in Fig. 1 and choose $\sigma_2 = 1$, $R_2 = 1$, and $\sigma_1 = \sigma$, $R_1 = R$. Let $\Phi_2(\theta)$ and $\Phi_1(\theta)$ denote the solutions for potential at the outer boundary $(R_2 = 1)$ for the cases where the inhomogeneity is and is not present, respectively. L_2 norm of the difference between the potentials Φ_1 and Φ_2, denoted by $||\Phi_d(\theta)||$, is the distinguishability measure defined by Isaacson [12].

In the eccentric inhomogeneity problem, the coil currents are the unknowns when one tries to maximize the distinguishability, and we need to maximize $||\Phi_d(\theta)||$ in the original problem domain. Let $\Phi_{t1}(\phi)$ and $\Phi_{t2}(\phi)$ denote the solutions for the electrostatic potential when the conductivity of inhomogeneity is one and σ, respectively, and consider the square of the L_2 norm of the difference voltage in w plane

$$||\Phi_d(\phi)||^2 = ||\Phi_{t1}(\phi) - \Phi_{t2}(\phi)||^2 = \int_0^{2\pi} (\Phi_{t1} - \Phi_{t2})^2 d\phi. \quad (21)$$

With the change of variable $\phi = \phi(\theta)$ we obtain

$$||\Phi_d(\phi)||^2 = \int_0^{2\pi} (\Phi_1(\theta) - \Phi_2(\theta))^2 |w'(z)||_{z=e^{j\theta}} d\theta \quad (22)$$

and using the mean-value theorem

$$\begin{aligned} ||\Phi_d(\phi)||^2 &= |w'(z)||_{z=e^{j\xi}} \int_0^{2\pi} (V_1(\theta) - V_2(\theta))^2 d\theta \\ &= |w'(z)||_{z=e^{j\xi}} ||\Phi_d(\theta)||^2 \end{aligned} \quad (23)$$

where $\xi \in (0, 2\pi)$. Hence, maximizing the voltage difference norm in the transform plane (ω) is equivalent to maximizing the voltage difference norm in the original (z) plane.

Collecting results from the previous parts, the objective function to be maximized during the distinguishability optimization is the magnitude of the following potential difference:

$$\Phi_2(\phi)-\Phi_1(\phi)=\sum_{m=1}^{M}\frac{-2\mu\rho_1^{m+1}}{1+\mu\rho_1^{2m}} \times\left\{\left[\rho_1^{m-1}C_m-E_m\right]\cos m\phi+\left[\rho_1^{m-1}D_m-F_m\right]\sin m\phi\right\}$$

where M is the number of terms kept in the Fourier series. Now the objective function will be expressed using the matrix or vector variables defined earlier.

Let R_a be a diagonal matrix representing coefficient ρ_1^{m-1} multiplying C_m. R_a can be written as

$$R_a=\begin{bmatrix}1 & 0 & \cdots\\ 0 & \rho_1 & \cdots\\ \vdots & \vdots & \vdots\\ 0 & \cdots & \rho_1^{M-1}\end{bmatrix}$$

and its size is $M\times M$. Similarly, define a diagonal matrix R_b as

$$R_b=\begin{bmatrix}\frac{-2\mu\rho_1^2}{(1+\mu\rho_1^2)} & 0 & \cdots\\ 0 & \frac{-2\mu\rho_1^3}{(1+\mu\rho_1^4)} & \cdots\\ \vdots & \vdots & \vdots\\ 0 & \cdots & \frac{-2\mu\rho_1^{M+1}}{(1+\mu\rho_1^{2M})}\end{bmatrix}.$$

Using these matrices the coefficients of $\cos m\phi$ can be written as

$$R_b(R_a\bar{C}-\bar{E})\bar{I}=X\bar{I}\text{ with }X=R_b(R_a\bar{C}-\bar{E})$$

and of $\sin m\phi$ can be written as

$$R_b(R_a\bar{D}-\bar{F})\bar{I}=Y\bar{I}\text{ with }Y=R_b(R_a\bar{D}-\bar{F}).$$

Now, distinguishability is maximized when $||XI||^2+||YI||^2$ is maximized. Note that these can be written as

$$\begin{aligned}||XI||^2&=I^TX^TXI\\ ||YI||^2&=I^TY^TYI.\end{aligned}$$

Therefore, optimization problem for limited peak coil current case can be given as

$$\text{Maximize}\quad I^T(X^TX+Y^TY)I \qquad \text{Subject to:}\quad |I_j|\le 1\text{ for every }j \quad (24)$$

and for the constant power constraint it becomes

$$\text{Maximize}\quad I^T(X^TX+Y^TY)I \qquad \text{Subject to:}\quad ||I||=\text{constant}. \quad (25)$$

As can be seen from the foregoing analysis, the optimization problem is solved by defining every parameter related in matrix or vector form. The forward problem solution is obtained in the same manner as explained in distinguishability optimization, the main difference being the currents are known in the forward problem. The modular structure of the analysis method enables to analyze a given geometry and to save all related matrices and to use the same data for different coil currents.

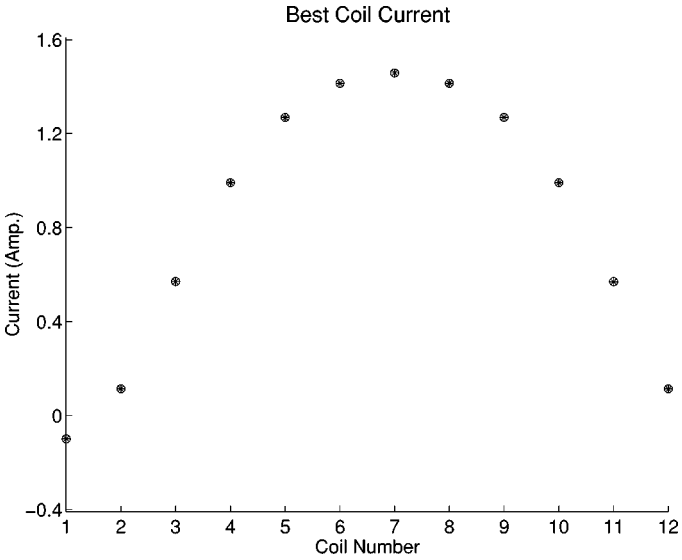

Fig. 3. Best coil currents found for example 1 under $||I||=\sqrt{12}$ constraint.

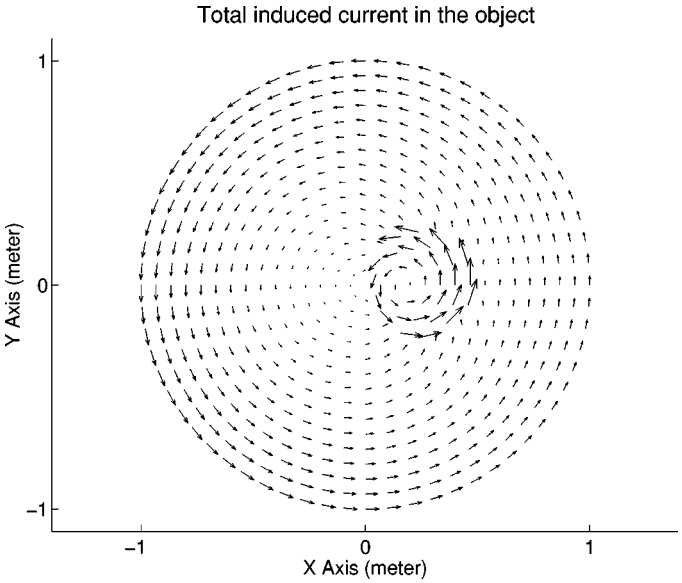

Fig. 4. Spatial distribution of total induced current in the object for example 1 when the best currents under $||I||=\sqrt{12}$ constraint are applied.

IV. Results

A 12-coil system is used for all examples given in this section for the investigation of eccentric inhomogeneity case. The operating frequency of the system is assumed as $f=50$ kHz.

As a first example, $R_1=0.25$ m, $R_2=1$ m, $\sigma_1=10$ S/m and $\sigma_2=1$ S/m with $c=0.25$ m are chosen. This corresponds to an inhomogeneity which is a good conductor. In order to have less than 1% error in the Fourier sum, 11 Fourier coefficients are needed in this example. The constant in the constraint is chosen as $\sqrt{N}=\sqrt{12}$ so that the current found would have the same power as the opposite drive and the comparison of the two would be meaningful. The best coil excitation currents under $||I||=\sqrt{12}$ constraint are

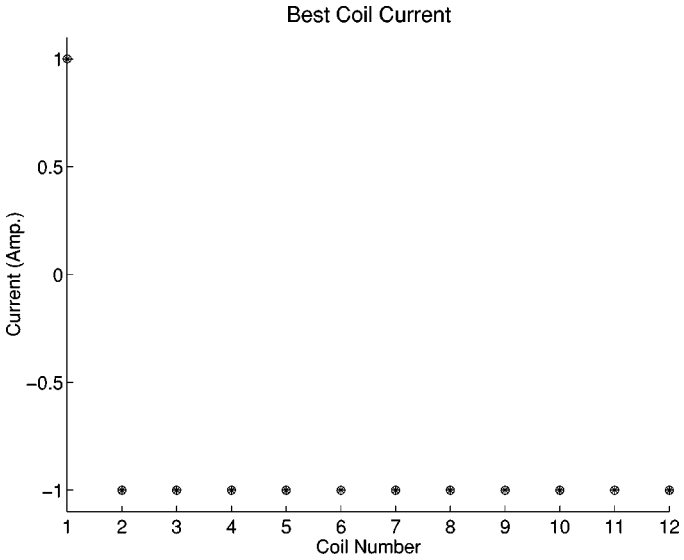

Fig. 5. Best coil currents found for example 2 under $|I_j| \leq 1$ constraint.

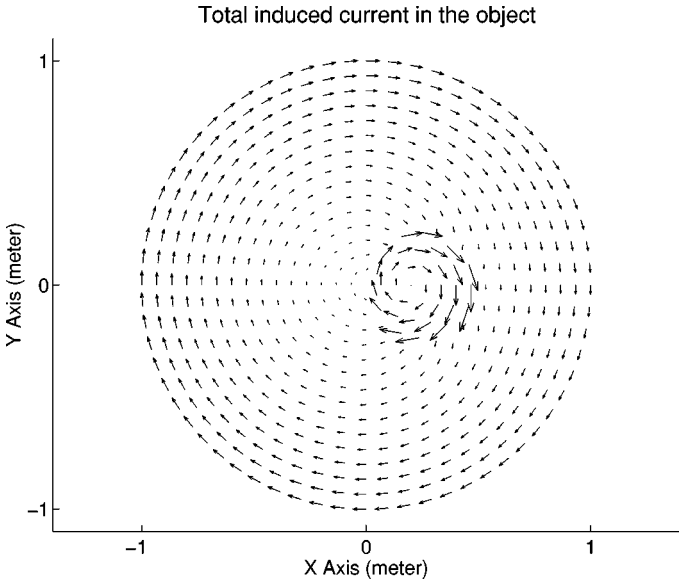

Fig. 6. Spatial distribution of total induced current in the object for example 2 when the best currents under $|I_j| \leq 1$ constraint are applied.

found as $I = [-0.0995\ 0.1139\ 0.5702\ 0.9912\ 1.2690\ 1.4145\ 1.4585\ 1.4144\ 1.2691\ 0.9911\ 0.5701\ 0.1138]$. The plot of coil currents as a function of coil number is shown in Fig. 3. It may be observed from the pattern of the current that it tries to locate the inhomogeneity. The induced current density in the object, when these optimum coil currents are used, is shown in Fig. 4. Maximum current density for this case is 73.8 mA/m. The directions of the arrows in Fig. 4 show the direction of the current and the lengths of the arrows are proportional to the magnitude of current at that location. The current is focused on the inhomogeneity as can be seen clearly in this figure. Earlier results [10] have shown that the best current pattern is a cosine drive for the concentric case. In the eccentric case the best current pattern resembles the sampled back-transform of the cosine drive. This observation brings about an extension of authors' earlier findings on optimum continuous injected-current patterns in [16] to discrete coil induced-current case. Choosing different drive axis location relative to the axis of inhomogeneity in the transform (ω) plane many different optimum current patterns can be obtained for the original problem in the z plane. Although the optimal currents will be different in the z plane, they would be all optimal in the sense that they give the same distinguishability. The reason for this is that they will all be obtained as sampling of the back transformation of the same current pattern in the ω plane.

For the second example, the problem defined in example 1 is solved under $|I_j| \leq 1$ constraint. The resulting current vector after the optimization is $I = [1\ -1\ -1\ -1\ -1\ -1\ -1\ -1\ -1\ -1\ -1\ -1]$ which is clearly related to an opposite drive formed by the coil currents. The current distribution for this example is given in Fig. 5. The total induced current density in the object is shown in Fig. 6. In this case the maximum is 70.8 mA/m and again the current is maximized on the inhomogeneity which is a sign of better distinguishability.

The third example has the same geometry as the previous examples but this time $\sigma_1 = 0$ S/m is chosen which corresponds to an insulator inhomogeneity. The best currents for limited peak

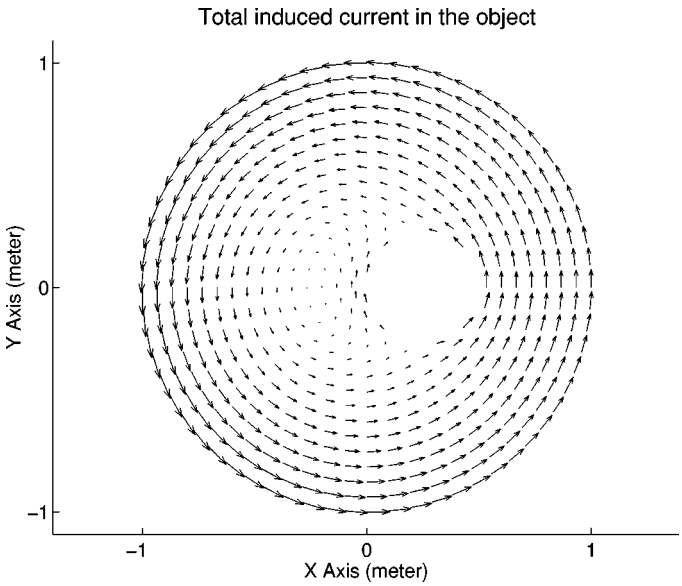

Fig. 7. Spatial distribution of total induced current in the object for example 3 when the best currents under $\|I\| = \sqrt{12}$ constraint are applied.

coil current and constant power constraints are the same as examples 2 and 1, respectively. This result reassures the trust in the best current results since the best current pattern must depend on the geometry of the problem, but not on the conductivity of the inhomogeneity. Total induced current for this example under constant power constraint has 41.8 mA/m as maximum value and its plot is given in Fig. 7. In this figure, the current is maximized along an axis and tangential currents at the boundary of the inhomogeneity are maximized.

Minimum detectable object radii are investigated next as a function of the location of the inhomogeneity center. For this purpose, again a 12-coil system is used and $\sigma_1 = 0$ S/m and $\sigma_1 = 10$ S/m cases are studied. For these two inhomogeneity conductivity levels, the performances of opposite drive and cosine drive are compared as the location of the inhomogeneity

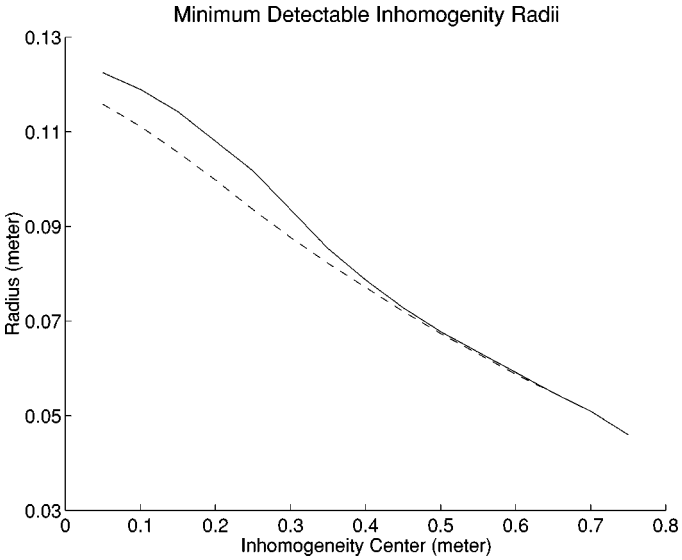

Fig. 8. Variation of minimum detectable inhomogeneity radii with c, (σ = 10 S/m, —: $|I_j| \leq 1$, – –: $\|I\| = \sqrt{12}$).

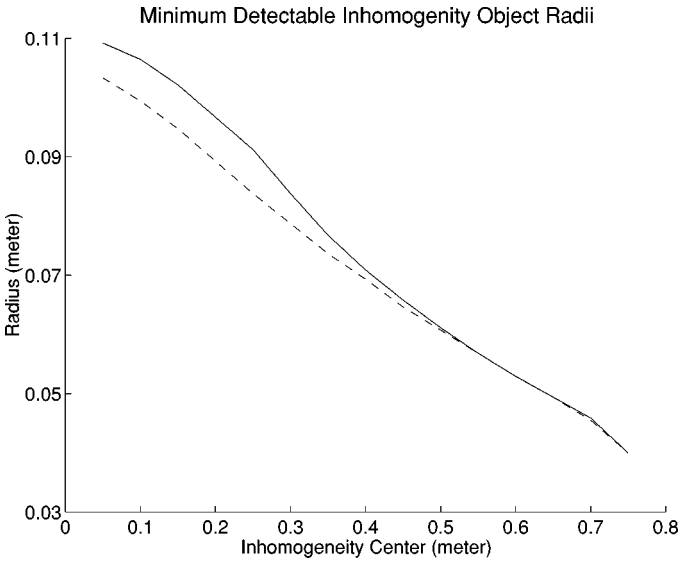

Fig. 9. Variation of minimum detectable inhomogeneity radii with c, (σ = 0 S/m, —: $|I_j| \leq 1$, –.–: $\|I\| = \sqrt{12}$).

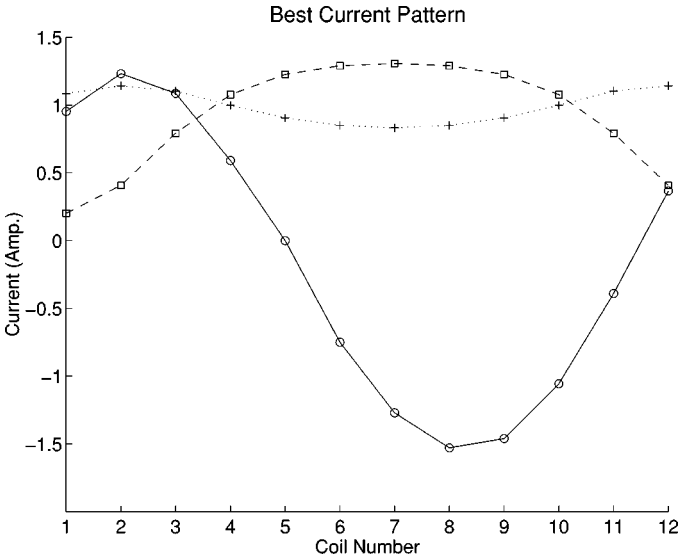

Fig. 10. Variation of best current pattern with c under $\|I\| = \sqrt{12}$ constraint, (—: $c = 0.05$ m, – –: $c = 0.4$ m, …: $c = 0.7$ m).

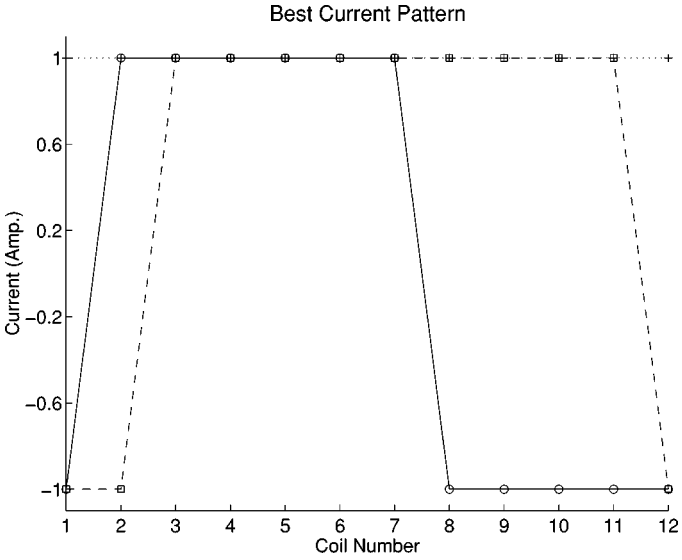

Fig. 11. Variation of best current pattern with c under $|I_j| \leq 1$ constraint, (– –: $c = 0.05$ m, – –: $c = 0.2$ m, …: $c = 0.6$ m).

center moves along the positive x axis. Although the calculation here is similar to the concentric inhomogeneity problem [10], there is an important difference: The best current pattern changes as the radius and the location of the inhomogeneity changes. Due to this reason, the best currents must be found for each radius tried. When finding the minimum radii, the threshold value for the distinguishability is chosen as 3% of the L_2 norm of the boundary potential vector obtained when the inhomogeneity is not present. The results are shown in Figs. 8–11. Fig. 8 compares the performances of the constant power and limited peak coil currents, when the two currents have the same power for $\sigma_1 = 10$ S/m case. It can be easily seen from this figure that constant power currents can detect smaller size inhomogeneities. Fig. 9 shows the same comparison for $\sigma_1 = 0$ S/m case. In both of these examples, the minimum detectable object radius for the two constraints approach one another as the inhomogeneity gets closer to the object boundary. This result should be expected because the best current pattern for both constraints approaches a uniform distribution as the inhomogeneity gets very close to the object boundary. Note that the minimum detectable object radius defined here is a theoretical limit to the size of the smallest object which can be imaged under finite measurement precision. There are other limitations related to reconstruction algorithms used to reconstruct images from measured data. As a result of this fact, an object distinguishable based on the criteria discussed here may not be identified in a reconstructed image. Fig. 10 shows the variation of the best coil currents under constant power constraint for three different locations of the inhomogeneity. The best current pattern for $c = 0.7$ m is very close to a uniform distribution. Fig. 11 shows the best current variation for $|I_j| \leq 1$ constraint and displays again convergence to the uniform current pattern.

Considering the examples and results given in this work, the best currents for the eccentric inhomogeneity case can be predicted. In accord with [10], [12], [16], the best current pattern is related to cosine drive under constant power constraint, and to opposite drive under limited peak coil current cases. Therefore, the best currents in the original plane are obtained by the sampling of the back-transform of these distributions.

V. Conclusion

In this work, an induced-current EIT system with discrete coils is analyzed for the general case of an eccentric inhomogeneity. The analysis is carried out using quasi-static assumptions and Fourier series. The purpose of the discrete coil system is to able to make independent measurements without having to change the location of the coil(s) or the object under investigation. Representative forward problem solutions demonstrate that the system is actually able to focus the current on the inhomogeneity.

In the second part of the work the problem of finding the best currents, in the sense that the distinguishability is maximized, is studied. It is shown that the best current pattern is related to cosine drive when the power is limited, and to opposite drive when the peak coil current is limited. An interesting result in this part showed that the best coil current pattern approaches uniform distribution as the inhomogeneity gets close to the object boundary. This is explained using the fact that the coil currents sample the back-transform of cosine or opposite drive depending on the constraint. Since the coil lengths are finite, sharp peaks of currents cannot be modeled and uniform distribution gives a better distinguishability.

The method reported in this work can be applied to a certain class of coil configurations which assures that the scalar line integral of the normal component of magnetic vector potential around a closed-contour in the cross-sectional plane is zero. Furthermore, the quantities used in the method are all put in a matrix or vector form enabling easy and modular solution.

References

[1] R. P. Henderson and J. G. Webster, "An impedance camera for spatially specific measurements of the thorax," *IEEE Trans. Biomed. Eng*, vol. BME-25, pp. 250–254, Mar. 1978.

[2] K. Boone, D. Barber, and B. Brown, "Review imaging with electricity: Report of the European concerted action on impedance tomography," *J. Med. Eng. Technol.*, vol. 21, pp. 201–232, 1997.

[3] B. Rigaund and J. P. Morucci, "Bioelectrical impedance techniques in medicine part III: Impedance imaging first section: General concepts and hardware," *Crit. Rev. Biomed. Eng.*, vol. 24, no. 4–6, pp. 467–597, 1996.

[4] J. M. Scaife, R. C. Tozer, and I. L. Freeston, "Real and imaginary impedance images using induced currents," in *Proc. Annu. Int. IEEE-EMBS Conf.*, vol. 12, 1990, pp. 116–17.

[5] T. J. Healey, R. C. Tozer, and I. L. Freeston, "Impedance imaging of 3D objects using magnetically induced currents," in *Proc. 14th Annu. Int. IEEE-EMBS Conf.*, 1993, p. 1719.

[6] I. L. Freeston and R. C. Tozer, "Impedance imaging using induced currents," *Physiological Measurement*, vol. 16, no. Suppl. 3A, pp. 257–266, 1995.

[7] N. G. Gencer, "Electrical impedance tomography using induced currents," Ph.D. dissertation, Middle East Tech. Univ., Ankara, Turkey, 1993.

[8] N. G. Gencer, Y. Z. İder, and S. J. Willamson, "Electrical impedance tomography: Induced-current imaging achieved with a multiple coil system," *IEEE Trans. Biomed. Eng.*, vol. 43, pp. 139–149, Feb. 1996.

[9] A. Köksal and B. M. Eyüboğlu, "Optimum excitation coil current pattern for a discrete coil induced current EIT system," presented at the *Proc. 2nd EPSRC Engineering Network Meeting on Biomedical Applications of EIT*, London, U.K., 2000.

[10] B. M. Eyüboğlu, A. Köksal, and M. Demirbilek, "Distinguishability analysis of an induced current EIT system using discrete coils," *Phys. Med. Biol*, vol. 45, pp. 1997–2009, 2000.

[11] R. V. Churchill, *Complex Variables and Applications*. New York: McGraw Hill, 1974, ch. 8.

[12] D. Isaacson, "Distinguishability of conductivities by electric current computed tomography," *IEEE Trans. Med. Imag.*, vol. MI–5, pp. 91–95, 1986.

[13] M. Cheney and D. Isaacson, "Distinguishability in impedance imaging," *IEEE Trans. Biomed. Eng.*, vol. 39, pp. 852–860, Aug. 1992.

[14] B. M. Eyüboğlu and T. C. Pilkington, "Comments on distinguishability in electrical impedance imaging," *IEEE Trans. Biomed. Eng.*, vol. 40, pp. 1328–1330, Dec. 1993.

[15] B. M. Eyüboğlu and T. C. Pilkington, "Correction on 'Comments on distinguishability in electrical impedance imaging'," *IEEE Trans. Biomed. Eng.*, vol. 41, p. 505, May 1994.

[16] A. Köksal and B. M. Eyüboğlu, "Determination of optimum injected current patterns in electrical impedance tomography," *Physiolog. Meas.*, vol. 16, no. Suppl. 3A, pp. 99–109, 1995.

[17] W. R. B. Lionheart, J. Kaipio, and C. N. McLeod, "Generalized optimal current patterns and electrical safety in EIT," *Physiolog. Meas.*, vol. 22, pp. 85–90, 2001.